

RESEARCH ARTICLE

Rear cortex contraction aids in nuclear transit during confined migration by increasing pressure in the cell posterior

Jeremy Keys^{1,2}, Brian C. H. Cheung³, Margaret A. Elpers^{1,2}, Mingming Wu³ and Jan Lammerding^{1,2,*}

ABSTRACT

As cells migrate through biological tissues, they must frequently squeeze through micron-sized constrictions in the form of interstitial pores between extracellular matrix fibers and/or other cells. Although it is now well recognized that such confined migration is limited by the nucleus, which is the largest and stiffest organelle, it remains incompletely understood how cells apply sufficient force to move their nucleus through small constrictions. Here, we report a mechanism by which contraction of the cell rear cortex pushes the nucleus forward to mediate nuclear transit through constrictions. Laser ablation of the rear cortex reveals that pushing forces behind the nucleus are the result of increased intracellular pressure in the rear compartment of the cell. The pushing forces behind the nucleus depend on accumulation of actomyosin in the rear cortex and require Rho kinase (ROCK) activity. Collectively, our results suggest a mechanism by which cells generate elevated intracellular pressure in the posterior compartment to facilitate nuclear transit through threedimensional (3D) constrictions. This mechanism might supplement or even substitute for other mechanisms supporting nuclear transit, ensuring robust cell migrations in confined 3D environments.

KEY WORDS: Nucleus, Confined migration, Invasion, Cortex, Mechanobiology, Pressure

INTRODUCTION

The migration of cells through tissues is essential to many biological processes, including embryogenesis, immune surveillance, wound healing and cancer metastasis (Doyle et al., 2013; Yamada and Sixt, 2019). During in vivo migration, cells must navigate through extracellular matrix networks and layers of endothelial cells, which form constrictions as small as 1 to 2 µm in diameter (Bone et al., 2016; Khatau et al., 2012; Weigelin et al., 2012; Wolf et al., 2013), which is substantially smaller than the size of the cell and the nucleus. Although cells can readily alter their morphology through cytoskeletal reorganization to adjust to the size of the constriction, the deformation of the nucleus represents a unique physical challenge, as it is the largest and stiffest organelle in the cell (Khatau et al., 2012; Wolf et al., 2013; Caille et al., 2002; Denais et al., 2016; McGregor et al., 2016) Because of the size and stiffness of the nucleus, cells must generate substantial intracellular forces to deform the nucleus through the constrictions. The process of

¹Nancy E. and Peter C. Meinig School of Biomedical Engineering, Cornell University, Ithaca, NY 14853, USA. ²Weill Institute for Cellular and Molecular Biology, Cornell University, Ithaca, NY 14853, USA. ³Department of Biological and Environmental Engineering, Cornell University, Ithaca, NY 14853, USA.

*Author for correspondence (jan.lammerding@cornell.edu)

D J.L., 0000-0003-4335-8611

Handling Editor: Andrew Ewald Received 10 September 2022; Accepted 20 May 2024 deforming and moving the nucleus through these narrow spaces, henceforth referred to as 'nuclear transit', limits the rate at which cells migrate in confined three-dimensional (3D) environments (Wolf et al., 2013; Denais et al., 2016; McGregor et al., 2016; Davidson et al., 2015; Harada et al., 2014; Jayo et al., 2016; Rowat et al., 2013; Thomas et al., 2015; Yadav et al., 2018).

Various mechanisms have been proposed to explain how cells accomplish nuclear transit through confined environments (McGregor et al., 2016; Marks and Petrie, 2022). In neurons and developing muscle cells, the kinesin and/or dynein microtubuleassociated motors are crucial for nuclear movement as these act to apply forces to the nucleus via the linker of nucleoskeleton and cytoskeleton (LINC) complex (Kalukula et al., 2022; Wilson and Holzbaur, 2012; Zhu et al., 2017; Tsai et al., 2010; Wu et al., 2011). In other cell types, nuclear movement is primarily driven by actomyosin-mediated forces. One commonly described mechanism suggests that actomyosin and intermediate filaments at the front of the cell pull the nucleus forward (Jayo et al., 2016; Petrie et al., 2014; Davidson et al., 2020). Other studies have implicated pushing forces in the process, mediated through perinuclear actomyosin fibers, which wrap around the nucleus (Thomas et al., 2015), or Arp2/3mediated perinuclear actin polymerization (Thiam et al., 2016). Each of these mechanisms depends on physical connections between the nucleus and cytoskeleton. Another proposed mechanism suggests that the nucleus is pushed forward by contraction of actomyosin in the rear cortex of migrating cells (Lämmermann et al., 2008; Mistriotis et al., 2019; Lee et al., 2021; Hetmanski et al., 2019; Poincloux et al., 2011; Ju et al., 2023 preprint). Support for the nucleus being pushed from behind derives from the observation that cells migrating in 3D environments commonly accumulate actin in the trailing edge of the cell, and that contraction of the cell rear often precedes nuclear transit (Thiam et al., 2016; Lämmermann et al., 2008; Mistriotis et al., 2019; Hetmanski et al., 2019). However, functional evidence for this mechanism is still lacking, including how forces from the contraction of the rear cortex are transmitted to the nucleus. Finally, many cell lines have shown the ability to migrate using multiple modes, such as adhesion-independent 'amoeboid' migration and integrin adhesion-based 'mesenchymal' migration, depending on cellular contractility and environmental adhesiveness (Sahai and Marshall, 2003; Liu et al., 2015). This plasticity of migration modes suggests that it is possible that cells might similarly switch between nuclear transit mechanisms in differing biological contexts (Marks and Petrie, 2022), but experimental evidence for this has been lacking. Thus, despite extensive previous research, several questions remain regarding the potential mechanism cells use to apply cytoplasmic forces to the nucleus during confined migration, including (1) how forces are transmitted from the contracting cell rear to the nucleus, and (2) to what extent contraction of the cell rear contributes to or is necessary for nuclear transit through small constrictions. Using microfluidic devices that mimic confined interstitial spaces, along with advanced

imaging and cellular manipulation approaches, we here describe a mechanism by which actomyosin in the rear cortex contracts to push the nucleus forward through constrictions. This mechanism is associated with enrichment of actin and active myosin in the rear cell cortex and depends on elevated RhoA–ROCK signaling. RhoA–ROCK-mediated contraction of the rear cortex results in elevated intracellular pressure in the posterior compartment of the cell, which pushes the nucleus from behind to support migration through confined spaces.

RESULTS

Contraction of the posterior actin cortex promotes nuclear transit through constrictions

To model cell migration through confined environments, we seeded cells into microfluidic devices that enable the close observation of nuclear transit through precisely defined constrictions at high spatiotemporal resolution (Davidson et al., 2015; Keys et al., 2018). In these devices, cells migrate through collagen-coated channels with constrictions measuring 1 to 2 µm in width and 5 µm in height (i.e. cross-sectional area $\leq 2 \times 5 \,\mu\text{m}^2$), formed by poly-dimethyl siloxane (PDMS) pillars (Fig. 1A). The devices also feature wider control channels (cross-sectional area $15 \times 5 \mu m^2$) that do not require substantial nuclear deformation during migration (Fig. 1A) (Davidson et al., 2015). The size of the narrow constrictions reflects the geometries of small pore sizes that migrating cancer cells encounter in vivo (Weigelin et al., 2012), whereas the width of the control channels was chosen to be wider than the typical diameter of nuclei (Lammerding, 2011) and corresponds to the upper range of interstitial spaces (Weigelin et al., 2012). We have previously demonstrated that the 5 µm height is sufficient to vertically confine migrating cells, and that cells adhere to both top and bottom surfaces of the cell, plus the vertical walls (Davidson et al., 2015, 2014),

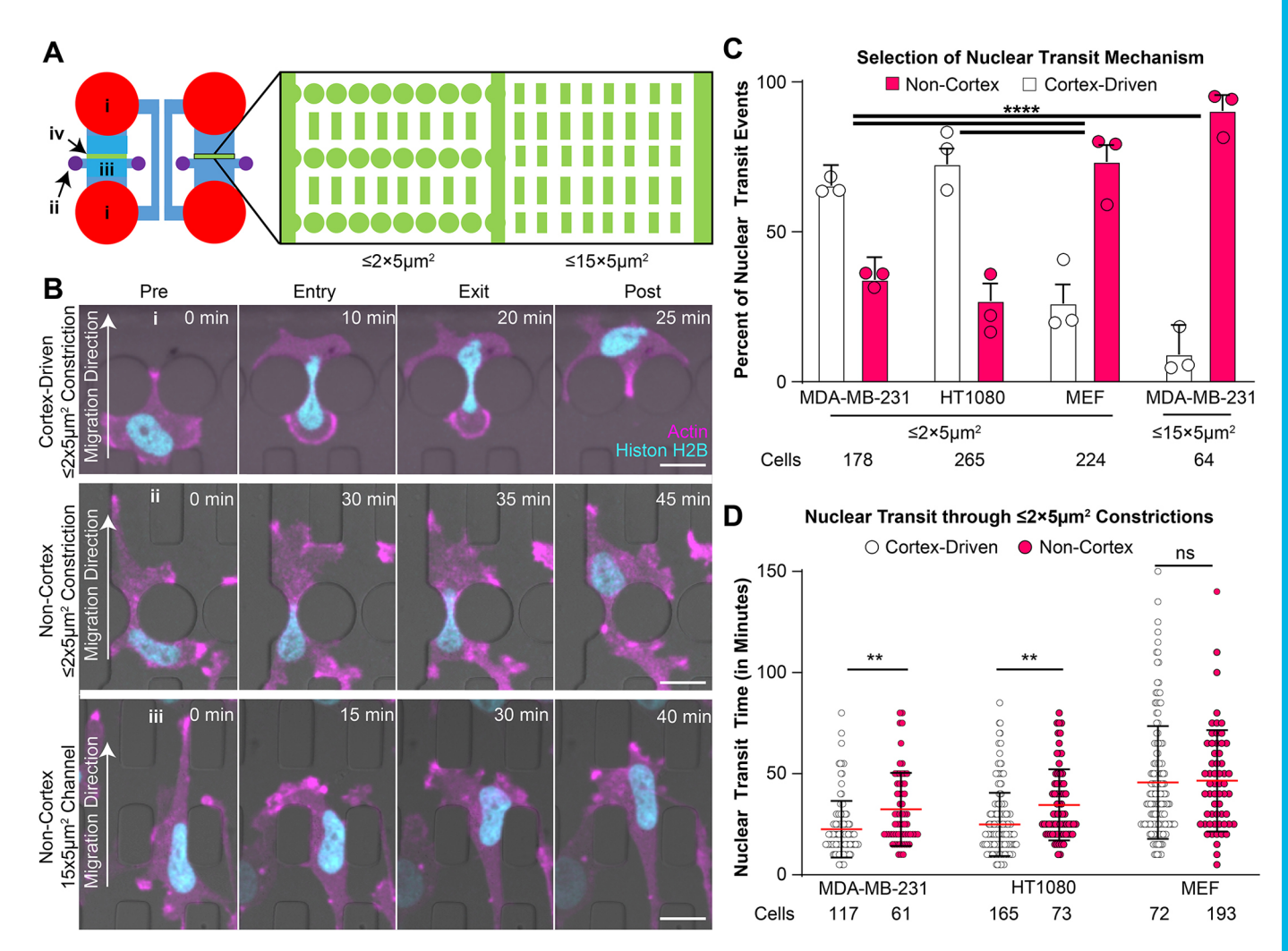


Fig. 1. Cortex-driven nuclear transit provides an advantage to cells migrating through narrow constrictions. (A) Schematic layout of microfluidic device used to study confined migration through precisely defined constrictions. (i) Reservoirs for cell media; (ii) seeding ports to add cells; (iii) seeding area where cells attach prior to migration through constrictions; (iv) constriction area, shown in detail in inset, to the right. The inset shows areas with constrictions (left) and the larger control channels (right), with the corresponding cross-sections listed below each area. (B) Representative image sequences of MDA-MB-231 cells co-expressing fluorescently labeled histones (mNeonGreen–H2B, cyan) and actin (mCherry2–actin chromobody, magenta). MDA-MB-231 cells adopt varying morphological characteristics as the nucleus squeezes through microfluidic constrictions using either (i) a rear cortex-driven mechanism, or (ii) a non-cortex driven mechanism. Scale bar: 20 μ m. (C) Relative frequency of cortex-driven and nuclear transit mechanisms in the different cell types migrating through either narrow constrictions (\leq 2×5 μ m²) or wider control channels (15×5 μ m²). Error bars represent 95% c.i. ****P<0.0001 (χ ² test of independence). Circles represent means of experimental replicates. (D) Nuclear transit times through \leq 2×5 μ m² constrictions for different cell types, subdivided into cortex-driven and non-cortex driven nuclear transit mechanisms. Red line represents sample mean. Error bars represent s.d. **P<0.01; ns, not significant (one-way ANOVA with Sidak's post test).

thereby creating true 3D confined environments that model confined migration *in vivo* (Denais et al., 2016; Wang et al., 2021). These devices provide several advantages over imaging cells migrating through collagen matrices, as they enable long-term imaging of cells migrating along a single focal plane, through precisely defined constriction geometries. In contrast, *in vitro* assembled collagen matrices have heterogeneous, randomly distributed constriction geometries and often lead to cells migrating out of the imaging plane during prolonged image acquisition series.

We chose to study MDA-MB-231 metastatic breast cancer cells because they exhibit the ability to switch between different migration modes (Sahai and Marshall, 2003; Geiger et al., 2019) and therefore might use multiple mechanisms to drive nuclear transit, MDA-MB-231 cells stably expressing fluorescently labeled histones (mNeonGreen-histone H2B; Davidson et al., 2015) and actin (mCherry2-actin chromobody; Chromotek) exhibited two distinct patterns of actin accumulation around the nucleus while migrating through constrictions in microfluidic migration devices. Most cells formed a rounded, actin-enriched cortex in the rear of the cell, the contraction of which was associated with the nucleus squeezing through the constriction (Fig. 1Bi; Movie 1, Fig. S1B–F). In other cells, the nucleus transited through the constriction without the cell forming a rounded rear cortex (Fig. 1Bii; Fig. S1G-I). Notably, whereas the formation of a distinct, rounded rear cortex was observed in the majority of MDA-MB-231 cells migrating through narrow constrictions, it was rarely observed in cells migrating through the larger control channels nor in cells migrating on 2D glass substrates (Fig. 1Biii,C; Fig. S2C). We observed similar patterns of actin accumulation at the rear of MDA-MB-231 cells migrating through 3D collagen matrices (Fig. S2D,E). Together with previous observations of the formation of a rounded rear cortex in MDA-MB-231 cells during transendothelial migration (Chen et al., 2016), our results indicate that these nuclear transit mechanisms are relevant during migration in physiological environments.

We hypothesized that the differences in cytoskeletal organization prior to and during nuclear transit indicate two distinct nuclear transit mechanisms, which might correspond to the previously described 'pushing' and 'pulling' forces. Accumulation of actin in the rear cortex suggests a 'cortex-driven' pushing of the nucleus from behind, whereas accumulation of actin in front of the nucleus suggests 'non-cortex-driven' pulling at the front of the nucleus. We recorded similar actin dynamics in HT1080 fibrosarcoma cells in microfluidic migration devices (Fig. 1C; Fig. S2B), another cancer cell line that shows considerable plasticity in its migratory mode (Wolf et al., 2003; (Petrie et al., 2016). In contrast, mouse embryonic fibroblasts (MEFs), which tend to use a mesenchymal migration mode (Gadea et al., 2007), predominantly used a non-cortex driven nuclear transit mode (Fig. 1C; Fig. S2A, Movie 2).

Based on these observations, we hypothesized that the rear cortex contraction aids MDA-MB-231 and HT1080 cells in nuclear transit through narrow constrictions by applying 'pushing' forces to the nucleus from the back of the cell. To determine whether the rear cortex contraction produced more rapid nuclear transit, we compared the transit times between cells using either (rear) cortex-driven or non-cortex driven nuclear transit for each of the cell lines. In MDA-MB-231 and HT1080 cells, cortex-driven cells translocated their nuclei significantly faster through narrow constrictions than non-cortex-driven cells (Fig. 1D), suggesting that, in these cell types, the rear cortex contractions provide an advantage over non-cortex driven migration. In contrast, we did not

find any differences in nuclear transit time between MEFs using the cortex versus the non-cortex driven mechanism (Fig. 1D). The preference towards a cortex-driven mechanism seen in MDA-MB-231 and HT1080 cells, in contrast to MEFs, might be due to the greater migratory plasticity that is commonly observed in these cancer cell lines (Sahai and Marshall, 2003). As MDA-MB-231 and HT1080 cells are capable of migrating using both mesenchymal and amoeboid migration modes, depending on environmental and biological factors, they might be able to use this additional cortexdriven nuclear transit mechanism to support passage through narrow constrictions. MEFs, in contrast, are more conventionally mesenchymal in their migration (Gadea et al., 2007), and therefore might be less able to use this additional migration mechanism. Taken together, these results suggest that rear cortex contraction acts as an alternative or supplemental mechanism in confined migration, which enables more rapid migration through constrictions but is not necessarily required for nuclear transit.

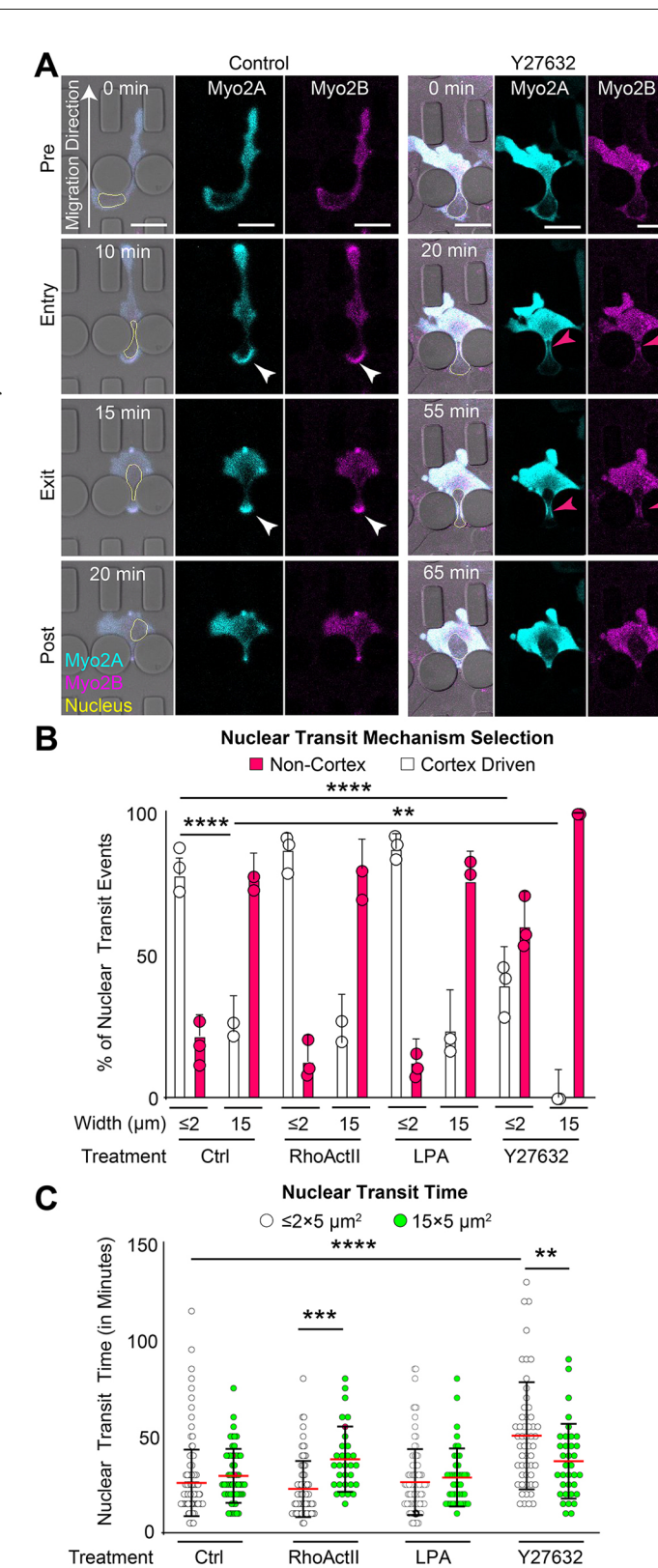
Given that previous studies had suggested that pulling forces at the leading edge of the nucleus require connections between the nucleus and cytoskeleton (Petrie et al., 2014; Davidson et al., 2020), we investigated whether disruption of the LINC complex caused a switch to a cortex-driven nuclear transit mechanism. We therefore chose to use MEFs as a model system, as we had previously observed them to primarily use a non-cortex driven migration mode. MEFs in which endogenous nesprin-2 (also known as SYNE2) was tagged with GFP (GFP–Nesprin-2, Davidson et al., 2020) and expressing an mCherry2-actin chromobody were modified to additionally express either a blue fluorescent protein (BFP) or a BFP-tagged dominantnegative KASH construct (DN-KASH), which binds with Sun proteins at the nuclear envelope and prevents the association between Sun proteins and endogenous nesprin proteins, thereby disrupting force transmission between the cytoskeleton and nucleus (Lombardi et al., 2011). Whereas GFP-Nesprin-2 was localized to the nuclear envelope in non-modified cells and in cells expressing a BFP-only control constructs, in DN-KASH-expressing MEF cells, nesprin-2 was mis-localized from the nuclear envelope (Fig. SS3A,B), confirming disruption of the LINC complex by the DN-KASH construct. Surprisingly, LINC complex disruption did not correspond with increased nuclear transit times nor with a shift towards a cortex-driven mechanism (Fig. S3C,D).

To determine whether these trends were cell line specific, we modified MDA-MB-231 cells to express either the doxycycline inducible DN-KASH construct or a BFP-only control. Similar to the results in the MEFs, DN-KASH expression resulted in endogenous nesprins (here, nesprin-1) being mislocalized from the nuclear envelope (Fig. S3E,F). DN-KASH expression did not significantly alter the proportion of cells employing cortex-driven versus noncortex driven migration modes (Fig. S3G), consistent with the results in MEFs (Figs. S3D). However, whereas DN-KASH expression had no effect on the nuclear transit times of MDA-MB-231 cells using cortex-driven migration, DN-KASH expression slowed the nuclear transit rate of MDA-MB-231 cells with noncortex driven migration (Fig. S3H). This increase in nuclear transit time upon LINC complex disruption differed from the results in MEFs, where LINC complex disruption had no effect on nuclear transit time (Fig. S3C). Collectively, these findings indicate that although some non-cortex-driven cells might require the LINC complex for efficient nuclear transit, the LINC complex is dispensable for cortex-driven nuclear transit. As this effect was only observed in one of the two tested cell lines, the precise requirements of the LINC complex for non-cortex-driven nuclear transit remains to be explored in future studies.

Rear cortex-driven nuclear transit is associated with actin and myosin II accumulation at the rear cortex and is dependent on RhoA-ROCK activity

We hypothesized that cortex-driven cells localize contractile machinery to the rear cortex to push the nucleus through constrictions. Previous studies have found that non-muscle myosin II is important for force generation during 3D confined migration (Thomas et al., 2015; Davidson et al., 2020); thus, we performed timelapse video microscopy on MDA-MB-231 cells transfected to transiently express GFP-myosin IIA and mCherrymyosin IIB in the migration devices. Both myosin II isoforms localized to the rear cortex of cells as the nucleus squeezed through constrictions (Fig. 2A; Fig. S1J–Q). Notably, the accumulation of myosin II at the rear cortex was only observed in cells migrating through narrow constrictions, whereas in cells migrating through larger control channels or on 2D surfaces, i.e., in situations not utilizing rear-cortex driven nuclear transit, myosin II was localized to the front of the cell body or the leading edge of the nucleus (Fig. 2A; Fig. S1R,S). Our studies also revealed that individual cells could switch between non-cortex-driven and cortex-driven mechanisms during nuclear transit. In some instances, cells that entered constrictions with GFP-myosin II initially primarily localized at the leading edge of the nucleus failed to pass through constrictions. When the nuclear transit attempt was not successful, the cells backed out of the constriction, and re-entered the constriction with GFP-myosin IIA localized to the rear cortex, using rear cortex contraction to successfully push the nucleus through the constriction (Movie 3). These findings suggest that cells can actively switch between nuclear transit modes while squeezing through small constrictions. In our analysis, out of 40 cells that completed multiple nuclear transits within the recorded timelapse sequence, nine cells (22.5%) 'switched' between nuclear transit mechanisms during successive nuclear transit events.

Given that myosin contractility is regulated through RhoA and Rho-associated protein kinase proteins 1 and 2 (hereafter generically denoted ROCK) (Ridley et al., 2003), we hypothesized that cells locally activate RhoA in the rear cortex to generate actomyosin contractile forces to push the nucleus from behind. To record the spatiotemporal dynamics of RhoA activation during nuclear transit, we stably modified MDA-MB-231 cells with a previously established fluorescence resonance energy transfer (FRET)-based biosensor for RhoA activity (Pertz et al., 2006) and imaged the cells as they migrated through constrictions. Local RhoA activity was determined by measuring the average FRET ratio in either the rear cortex, front cortex or directly in front of the nucleus (Fig. S4A). Given that levels of the RhoA sensor inside the nucleus were very low, as expected, which could negatively affect the robustness of ratiometric FRET analysis, the nucleus was masked-out and excluded from the analysis (Fig. S4A). FRET ratios of the RhoA biosensor were evaluated prior to nuclear transit ('Pre'), during nuclear entry into a constriction ('Entry'), immediately upon nuclear exit from the constriction ('Exit') and after the cell had left the constriction ('Post') (Fig. 3A). Consistent with prior reports (Pertz et al., 2006), RhoA activity was increased at the leading edge of the migrating cells (Fig. 3A). However, as cells migrated through narrow constrictions, RhoA activity in the rear cortex became elevated relative to other regions within the cell during nuclear transit (Fig. 3B). This increase in RhoA activity in the rear cortex was unique to cells migrating through narrow 3D constrictions and was not observed in cells migrating through the wider control channels or on 2D substrates (Fig. S4B). In confined conditions,



RhoA activity in the rear cortex increased as the nucleus entered the constriction and then returned to baseline levels during the later stages of nuclear transit (Fig. 3C). Unlike RhoA activity at the rear cortex, RhoA activity at the leading edge of the

96 42

53 35

78 31

Cells

147 56

During Nuclear Transit

1.2

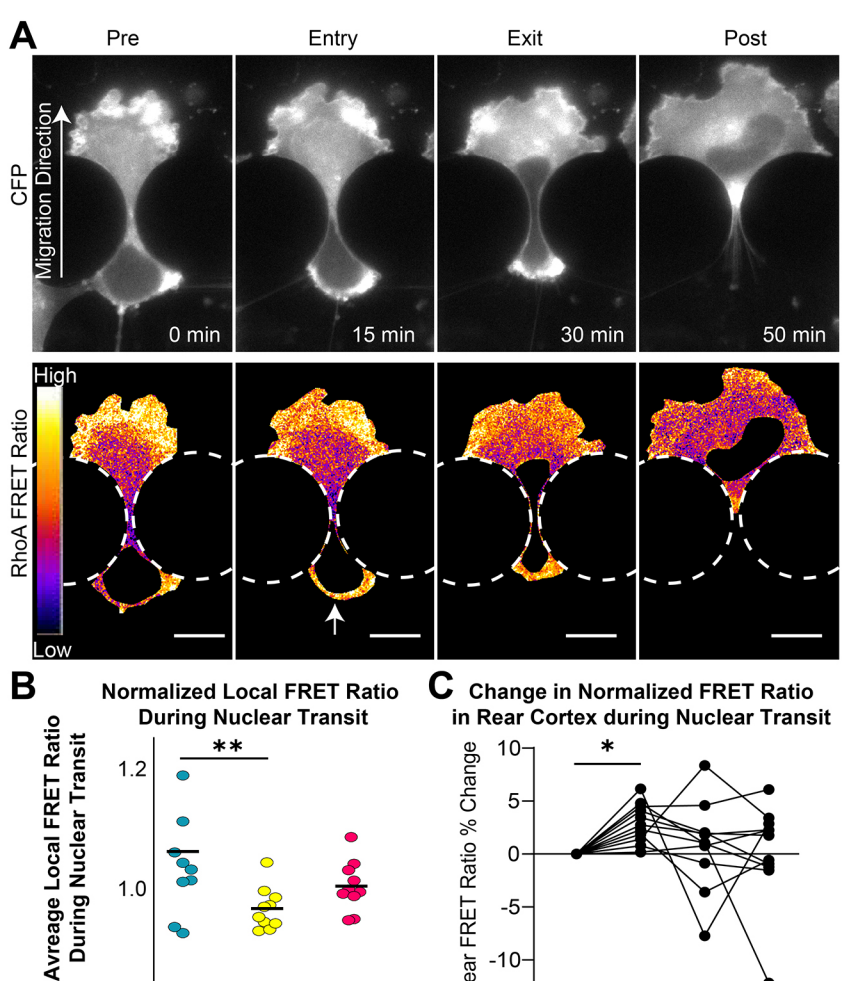
1.0

Fig. 2. Rear cortex driven nuclear transit is associated with localization of myosin II to the rear cortex. (A) Representative time-lapse series of MDA-MB-231 cells expressing GFP-myosin IIA and mCherry-myosin IIB migrating through microfluidic migration devices. White arrowheads indicate accumulation of myosin II at the rear cortex. Magenta arrows point to accumulation in front of the nucleus. The nucleus is outlined in yellow for better visibility in the merged image. Scale bars: 20 µm (B) Percentage of nuclear transit events using cortex-driven or non-cortex driven modes in either ≤2×5 µm² or 15×5 µm² constrictions following treatment with either RhoA activators (RhoActII or LPA), ROCK inhibitor (Y27632) or vehicle control. Error bars represent 95% c.i. **P<0.01; ****P<0.0001 (χ^2 test of independence). Circles represent mean of each experimental replicate. (C) Nuclear transit times of MDA-MB-231 cells migrating through constrictions following treatment with RhoA activators (RhoActII or LPA) or ROCK inhibitor (Y27632). Red line represents mean. Error bars represent s.d. Number of cells in each group indicated below the graphs. **P<0.01; ***P<0.001; ****P<0.0001 (one-way ANOVA with Sidak's post test).

cell remained constant throughout nuclear transit (Fig. S4D). RhoA activity in front of the nucleus (Fig. S4A, yellow zone) did not increase upon nuclear entry into the constriction but increased at the end of nuclear transit (Fig. S4C). Collectively, these observations suggest a sequential process in which RhoA is first activated at the posterior of the cell, causing contraction of actomyosin in the rear cortex to push the nucleus into a

constriction, followed by activation of RhoA in front of the nucleus to contract actomyosin at the leading edge of the nucleus to pull the nucleus through the constriction.

As the cortex-driven nuclear transit mechanism was associated with active RhoA and myosin II at the rear cortex, we hypothesized that the cortex-driven nuclear transit mechanism depends on Rho-ROCK activity. We treated cells with either ROCK inhibitor (Y27632) or RhoA activators (LPA or RhoA activator II) and measured nuclear transit times in the microfluidic devices. ROCK inhibitor treatment significantly slowed nuclear transit through the constrictions but did not slow migration through unconfined channels (Fig. 2C), suggesting that ROCK activity is particularly important for confined migration. Interestingly, ROCK inhibition increased the frequency of non-cortex driven nuclear transit events and altered localization of myosin IIA and IIB during nuclear transit, causing myosin to localize towards the front of the nucleus, rather than in the rear cortex as is seen in vehicle-only control cells (Fig. 2A,B). As ROCK inhibition slowed down nuclear transit through narrow constrictions but not through unconfined channels, these findings also suggests that the role of ROCK in pushing the nucleus from behind is unique to nuclear transit through narrow constrictions. This observation mirrors our earlier observation that cells in unconfined channels rarely use a cortex-driven migration



Rear FRET Ratio % Change

5-0

-5-

-15-

Pre Entry Exit **Nuclear Position**

Post

Fig. 3. Cortex-driven nuclear transit is associated with increased RhoA activity at the rear cortex. (A) Representative time-lapse series of FRET ratio of MDA-MB-231 cell expressing a RhoA-FRET biosensor migrating through a microfluidic constriction. The bottom series shows the RhoA-FRET ratio during nuclear transit, illustrating increased RhoA activity at the rear cortex (arrow) and the leading edge of the cell. Scale bars: 20 um (B) Comparison of RhoA activity at different intracellular locations based on the recorded RhoA-FRET values for cells migrating through \leq 2×5 μ m² constrictions. Each data point represents local RhoA FRET measurements averaged across all time points during a single nuclear transit event. Black lines represent the mean for each group. **P<0.01 (Friedman test). (C) Time course of FRET ratio within rear cortex of individual cells (normalized to average FRET ratio of whole cell) at each phase of nuclear transit through $\leq 2 \times 5 \mu m^2$ constrictions. *P<0.05 (Friedman test).

mode. Ectopic activation of RhoA with either LPA or RhoA activator II had no effect on the nuclear transit rate or nuclear transit mechanism in MDA-MB-231 cells (Fig. 2C), presumably due to the already abundant levels of LPA present in the serum. The lack of effect of pharmacological RhoA activators on nuclear transit rate or mechanism might indicate that RhoA in these cells is already highly activated by serum in the cell medium or that global RhoA activation without spatial control within the cell is insufficient to activate the cortex-driven transit mechanism. Although actomyosin contractility likely plays a role in both cortex-driven and non-cortex driven mechanisms, these results further suggest that cortex-driven nuclear transit requires a particularly high level of Rho–ROCK-mediated contractility in contrast to non-cortex driven nuclear transit.

Laser ablation of the cell cortex reveals a pressure-driven nuclear transit mechanism

Having established that cortex-driven cells localize actomyosin and active RhoA to the rear cortex at the beginning of nuclear transit, we hypothesized that contraction of the rear cortex pressurizes the rear compartment of the cell relative to the front compartment, pushing the nucleus forward through the constriction. To probe differences in intracellular pressure generated by rear cortex contraction, we used a two-photon laser to ablate specific cytoskeletal regions of migrating cells while they squeezed their nucleus through microfluidic constrictions (Fig. 4A; Fig. S5A). As the nucleus transits through a constriction, the cytoskeletal forces pushing or pulling on the nucleus are counteracted by the resistance of the constriction in the form of the friction and the normal forces at the interface between the nucleus and the constriction (Fig. S5B,C).

Targets for laser ablation were selected based on previously hypothesized roles in applying pushing or pulling forces on the nucleus during nuclear transit, including: (1) perinuclear actin filaments at the leading edge of the nucleus ('Nuclear Front'), which pull the nucleus forward, (2) the rear cortex, whose contraction pushes the nucleus from behind ('Rear'), (3) the front cortex at the leading edge of the cell, which might retain pressure in the front compartment of the cell that could inhibit nuclear transit ('Front'), (4) both cortexes simultaneously to compare compartmentalized pressure in the front and rear of the cell body ('Both'), and (5) non-ablated cells to control for spontaneous movement of the nucleus during experiments (Fig. 4A). If contraction of the rear cortex pushes the nucleus forward, then ablation of the rear cortex during nuclear transit is expected to result in the nucleus falling backwards (Fig. S5C). By contrast, if the nucleus is pulled forward by actomyosin fibers at the leading edge of the nucleus, as has been previously shown in MEFs (Davidson et al., 2020), then ablation at the nuclear front should result in the nucleus moving backwards (Fig. S5C). In contrast, ablation of the front cortex, which might inhibit forward movement of the nucleus through maintaining increased pressure in the front compartment of the cell (Petrie et al., 2014), is expected to result in forward movement of the nucleus (Fig. S5C). In all cases, movement of the nucleus in response to laser ablation is expected to occur almost instantaneously, as ablation should immediately disrupt the balance of forces acting on the nucleus, and nuclear movement will only be resisted by viscous forces within the cytoplasm (in the case of rearward movement) or the resistance of microfluidic constrictions (in the case of forward

As seen in previous studies (Mistriotis et al., 2019; Tinevez et al., 2009; Charras et al., 2005), ablation of the cell cortex caused the formation of a large plasma membrane bleb, indicating the release of cytosolic pressure (Fig. 4B, arrow). Ablation of the rear cortex and

formation of the bleb at the cell posterior led to transient rearward movement of the cell nucleus (Fig. 4B–D; Fig. S5D). This observation supports our hypothesis that contraction of the rear cortex pushes the nucleus from behind by increasing intracellular pressure in the rear compartment. Furthermore, recovery and contraction of the bleb within a minute of the initial laser ablation resulted in forward movement of the nucleus (Fig. 4B–D), indicating that restoration of the cell rear cortex increased intracellular pressure in the back of the cell and pushed the nucleus forward.

Following ablation of the front cortex of cells, the nucleus immediately moved forwards, suggesting that, prior to ablation, pressure in the front compartment of the cell impeded forward movement of the nucleus (Fig. 4C,D; Fig. S5A,D). However, the magnitude of the nuclear forward movement was less than the rearward movement observed when ablating the rear cortex, suggesting that pressure in the rear compartment might be greater than the pressure in the front compartment (Fig. 4C,D). To assess directly whether the pressure is greater in the rear compartment of the cell than in the front compartment, we ablated both front and rear cortexes of the cell simultaneously (Fig. 4C,D; Fig. S5D). Ablation of both cortexes led to a rearward shift of the nucleus, confirming that the pushing force generated by the pressure from the rear cortex contraction was greater than the resisting force generated by pressure from the front compartment (Fig. 4C,D).

As an additional means of comparing pressure between the front and rear compartments of the cell, we measured the size of blebs in the cell cortex formed as a result of cortex ablation (Fig. 4E). Previous work has demonstrated that bleb size following laser ablation increases as a consequence of elevated intracellular pressure and is limited only by the elasticity of the cell membrane (Tinevez et al., 2009). Thus, increased bleb sizes following laser ablation indicate increased intracellular pressure prior to ablation. Following simultaneous ablation of the front and rear cortexes, blebs formed in the rear compartment were significantly larger than blebs in the front compartment, indicating that pressure in the rear of the cell is greater than pressure in the front compartment (Fig. 4E). Collectively, these findings confirm that increased pressure at the cell rear helps to push the nucleus forward through constrictions.

Ablation directly in front of the nucleus led to a subtle rearward shift of the nucleus, suggesting the presence of pulling forces at the leading edge of the nucleus (Fig. 4B,C; Fig. S5A,D), consistent with previous findings (Davidson et al., 2020). However, the rearward movement of the nucleus was very modest in comparison to the movement following rear cortex ablation (Fig. 4D). These findings indicate that the cortex-driven cells relies more heavily on pushing forces from behind the nucleus than on pulling forces at the nuclear front, which is consistent with the faster nuclear transit we observed in the cells using the cortex-driven mechanism (Fig. 1D).

We hypothesized that these intracellular pressure-driven pushing forces resulted from the accumulation and contraction of actomyosin in the rear cortex during cortex-driven nuclear transit. As we observed that ROCK inhibition reduced myosin accumulation in the rear cortex, we hypothesized that ROCK inhibition reduces intracellular pressure behind the nucleus. Following Y27632 treatment, nuclear movement following rear cortex ablation was reduced, whereas nuclear shift in response to ablation of the nuclear front was unaffected (Fig. 4D), indicating that pushing forces between the rear cortex and nucleus result from ROCK-dependent actomyosin contractility. Additionally, ROCK inhibition led to a substantial decrease in the size of blebs formed following laser ablation (Fig. 4E), further confirming that ROCK-mediated actomyosin contractility drives contraction of the rear cortex and increased cytosolic pressure in the rear compartment of the cell.

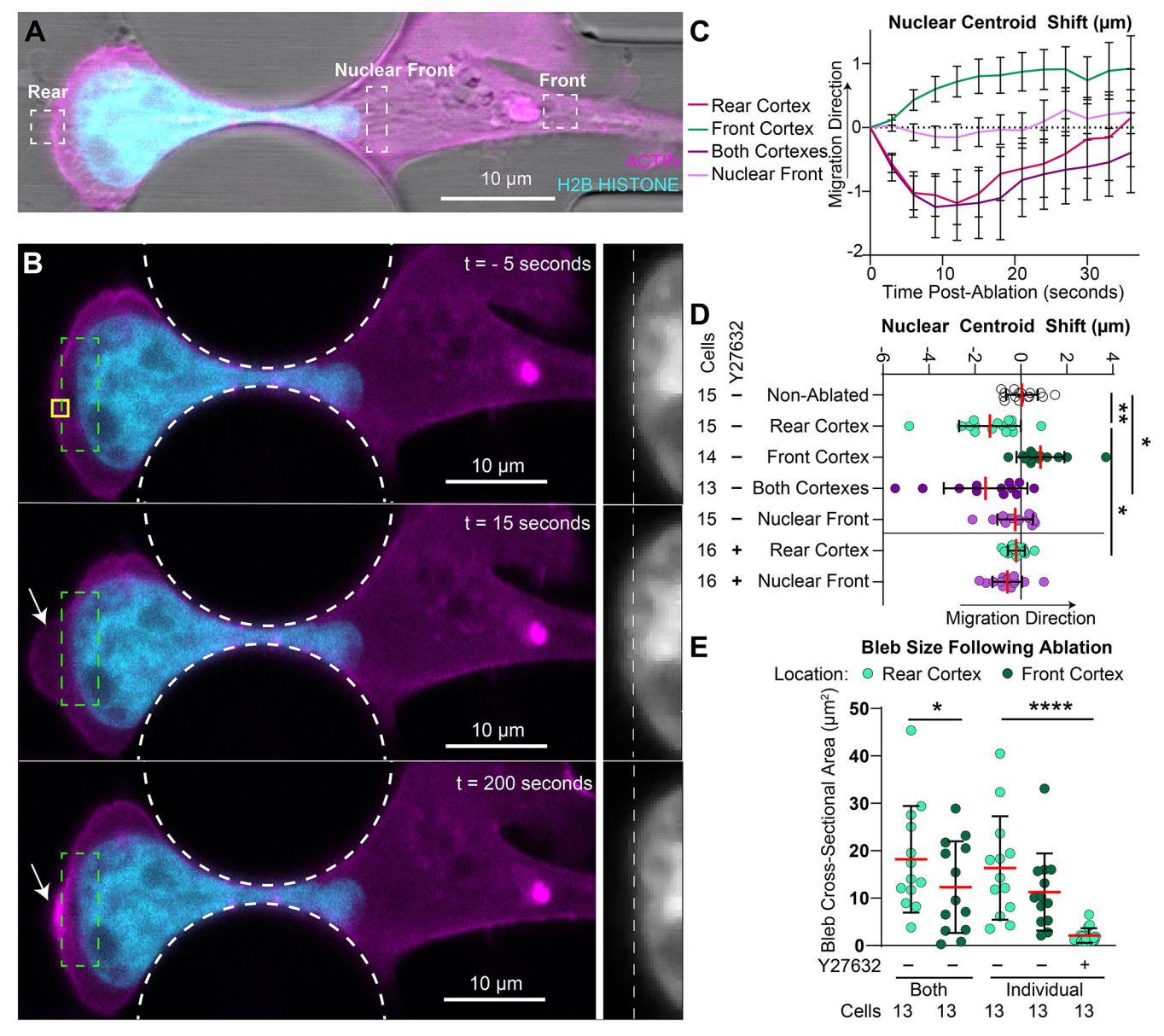


Fig. 4. Nuclear movement following laser ablation of local actin cytoskeleton reveals that cortex-driven nuclear transit results from increased pressure in the rear compartment. (A) Laser ablation set-up. Dashed boxes represent regions targeted for laser ablation in cells starting to undergo nuclear transit through a small ($\leq 2 \times 5 \mu m^2$) constriction. Cells were modified to stably express mNeonGreen—histone H2B and mCherry—actin chromobody to visualize nuclear movement and actin cytoskeleton, respectively. (B) Representative time-lapse series of cell ablated at the rear cortex. Yellow box represents laser ablation target. Arrow shows plasma membrane bleb formation post-ablation. Dashed green box denotes the location of the close-up with the mNeonGreen—histone H2B signal shown on the right. In the close-up on the right, the dashed white line represents starting point of leading edge of nucleus. (C) Trace of nuclear centroid shift following laser ablation. Error bars represents mean $\pm s$.e.m., based on 13–16 cells per condition. (D) Quantification of peak nuclear centroid shift immediately following nuclear ablation. Red line represents mean, black error bars represent s.d. *P<0.05; *P<0.01 (unpaired non-parametric Kruskal–Wallis test). (E) Cross-sectional area of blebs formed after cortex ablation. Cell counts per condition shown below graph. Red lines represent mean, black error bars represent s.d. *P<0.05 (Friedman test); *****P<0.0001 (unpaired non-parametric Kruskal–Wallis test).

DISCUSSION

In this study, we investigated the cytoskeletal dynamics and intracellular forces acting on the nucleus as cells migrate through confined spaces. We identified a mechanism by which contraction of actomyosin at the rear cortex pushes the nucleus through constrictions during 3D migration. Our results suggest that cortex-driven nuclear transit is a distinct mechanism from the alternative 'non-cortex-driven' mechanisms that have been described previously (Petrie et al., 2014; Davidson et al., 2020). In the cortex-driven nuclear transit mechanism, pushing forces at the cell rear are generated through contraction of

actomyosin in the posterior cortex, which elevates cytosolic pressure behind the nucleus to push the nucleus forwards (Fig. 5). This contrasts with the non-cortex-driven modes, in which pulling forces, through actomyosin or intermediate filaments, are mediated through physical connections between the nucleus and cytoskeleton (Thomas et al., 2015; Petrie et al., 2014; Davidson et al., 2020) (Fig. 5). Our studies suggest that some cell lines can use both mechanisms to achieve nuclear transit, although individual cell lines might have a propensity to use one mechanism over another. It remains to be elucidated whether these pushing and pulling mechanisms work

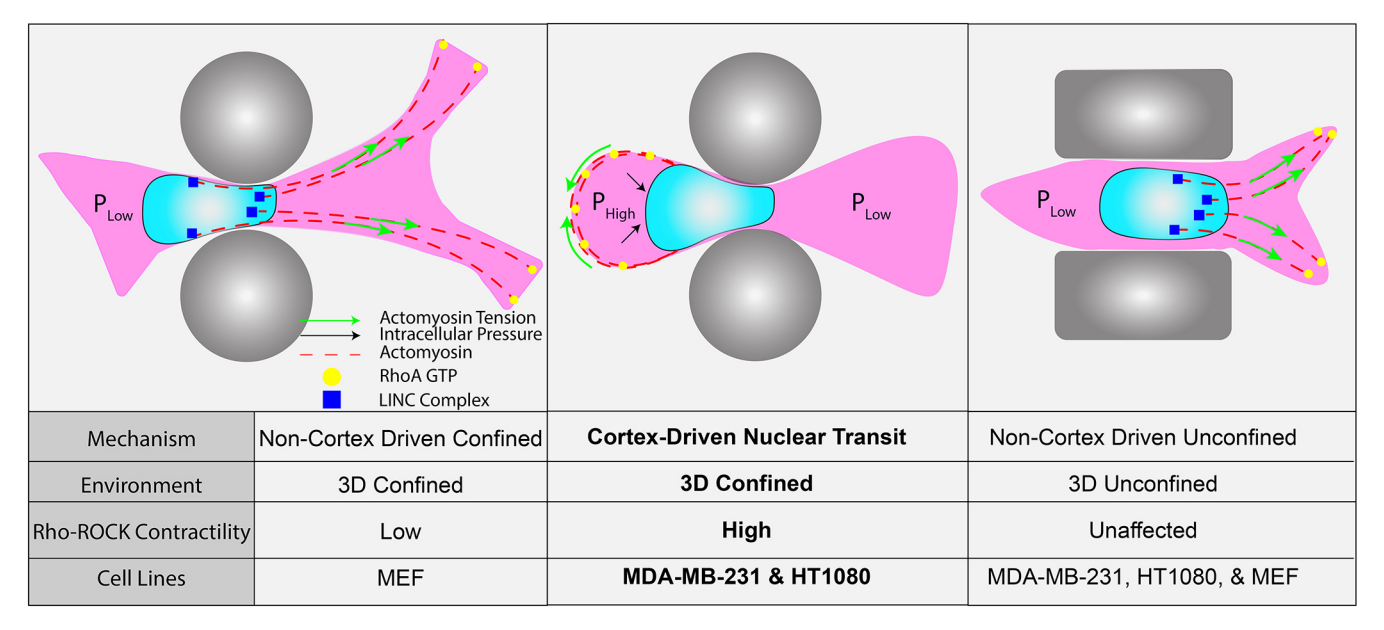


Fig. 5. Model of alternative mechanisms of nuclear transit through constrictions. Pushing forces are generated through contraction of the posterior cortex, caused by colocalization of active RhoA, myosin II and actin. Colocalization of these same proteins at the leading edge of the nucleus can generate pulling forces at the front of the nucleus, mediated through the LINC complex.

independently to accomplish nuclear transit, or whether they act complimentarily.

Mirroring our findings in microfluidic devices and collagen matrices, accumulation of actomyosin in the rear of cells migrating in 3D has been observed in MDA-MB-231 cells invading through Matrigel (Poincloux et al., 2011) and in vitro models of transendothelial migration (Chen et al., 2016), indicating that rear cortex-driven nuclear transit might play an important role in these physiological processes. Previous studies of 3D dendritic cell migration have reported that retraction of the cell rear precedes nuclear squeezing through constrictions (Lämmermann et al., 2008). These studies showed that inhibition of contractility through treatment with blebbistatin and Y27632 delayed contraction of the cell posterior, which corresponded with a reduced migration rate in confined environments (Lämmermann et al., 2008; Schaar and McConnell, 2005). However, it was unclear whether this retraction represented a direct transmission of force between the rear cortex and the nucleus or whether rear retraction followed the forward movement of the nucleus. More recent findings have found elevated RhoA activity and myosin at the rear of cells migrating through 3D channels and give evidence that this results in increased intracellular pressure behind the nucleus (Mistriotis et al., 2019). However, these studies did not address how intracellular pressure could contribute to nuclear transit through constrictions. Our results build upon these prior findings by confirming that retraction of the rear cortex pushes the nucleus forward during nuclear transit, and by demonstrating a functional role for cortex-driven pressure generation in confined 3D migration.

Our findings complement prior studies that have probed intracellular forces acting on the nucleus during cell migration. One such set of studies evaluated the role of pulling forces at the front of the nucleus, which increase intracellular pressure in the front compartment of fibroblasts and HT1080 cells migrating through 3D environments (Petrie et al., 2014, 2016). In contrast to our work, these studies used a probe to directly measure intracellular pressure in cells migrating through 3D cell-derived matrix. They found that actomyosin and intermediate filaments at the nuclear front pulled the nucleus forward to increase pressure at the leading edge of cells,

which generated 'lobopodia' to enable invasion through 3D environments. The apparent differences in the results might be due to the different cell types use or reflect differences in the geometry and physical properties of the microenvironment. For example, subsequent studies in mesenchymal stem cells migrating in 3D alginate hydrogels have indicated that pulling forces at the leading edge of the nucleus are not necessary for the formation of lobopodia (Lee et al., 2021). In the absence of nesprins, the nucleus was still able to move forward into constrictions to pressurize the front compartment of cells, and the authors noted an accumulation of phosphorylated myosin light chain in the rear cortex. These results mirror our findings of active RhoA in the rear cortex during nuclear entry to constrictions, supporting the idea that elevated pressure at the cell rear is increased at the beginning of nuclear transit.

One limitation of our studies is that our detection of intracellular forces must be inferred from protein localization and changes in nuclear position following laser ablation, rather than measuring these forces directly, as the PDMS enclosure of the microfluidic migration devices prevents direct access to the migrating cells. Our laser ablation assay is limited as an indirect measurement of intracellular pressure (or other cytoskeletal forces), as it only reveals forces acting on the nucleus at a single point in time, although the pressure throughout the cell body during nuclear transit might be highly dynamic as the nucleus shifts from the rear compartment of the cell to the front compartment. Additionally, the laser ablation likely disrupts not only actomyosin but also other force-generating cytoskeletal structures within the target region, including intermediate filaments and microtubules, which could further contribute to the force transmission and force generation. Nonetheless, as we found that the cortex-driven mechanism strongly depends on the Rho-ROCKmyosin pathway, we believe that this mechanism principally depends on actomyosin activity, though our results cannot rule out potential contributions of other cytoskeletal elements, which have previously been implicated in nuclear movement (Tsai et al., 2010; Petrie et al., 2014). In addition, the distinct circular shape of rear cortex, in contrast with that of front cortex, further supports the conclusion that the pressure is higher in the rear compartment.

A recent report has demonstrated the role of pulling forces in mediating nuclear transit in MEFs (Davidson et al., 2020). Similar to our results in MDA-MB-231 cells, the authors demonstrated that ROCK inhibition increases nuclear transit times of MEFs migrating through narrow constrictions, but not through unconfined 3D channels (Davidson et al., 2020). Using a laser ablation assay, as we have used here, they found that ablation in front of the nucleus caused a rearward shift in the nucleus whereas ablation at the cell rear had no effect on nuclear movement. They also found that the rearward shift in nuclear position following ablation at the nuclear front was dependent on connections between the nucleus and cytoskeleton. These results contrast with our data in MDA-MB-231 cells, as we detected only very subtle nuclear shifts following ablation of the nuclear front and a significant rearward shift of the nucleus after rear cortex ablation, and LINC complex disruption did not impede nuclear transit (Fig. S3). This difference in results could be attributable to our findings that MEFs rarely use the cortex-driven nuclear transit mechanism in comparison to MDA-MB-231 cells, which very frequently used the cortex-driven mode. These two findings are complementary in that they highlight a key difference between MEFs, which in the 'non-cortex-driven' mode apply pulling forces at the front of the nucleus (Davidson et al., 2020), and cortex-driven MDA-MB-231 cells, which push the nucleus from behind through intracellular pressure generated by the rear cortex.

In our studies using a dominant-negative nesprin construct (DN-KASH), LINC complex disruption had context-dependent effects on nuclear transit time. In MDA-MB-231 cells, DN-KASH expression did not alter nuclear transit times in cells using rear cortex-driven migration but increased nuclear transit times in cells using non-cortex-driven migration, suggesting that the LINC complex is important for pulling the nucleus forward. Surprisingly, DN-KASH expression did not significantly alter nuclear transit times in MEFs, suggesting cell-type-specific or context-dependent differences.

Although we have noted a cell-type-specific preference towards the cortex-driven mechanism, and that the mechanism depends on high Rho-ROCK-mediated contractility, it remains unclear which biological and/or environmental factors cause individual cells to adopt a particular nuclear transit mechanism. As others have found that pulling forces at the front of the nucleus depend on the LINC complex (Davidson et al., 2014; Petrie et al., 2016), it is possible that the cortex-driven mechanism could compensate for a lack of pulling forces in specific scenarios. For example, pulling forces at the leading edge of the cell require adhesions to the surrounding environment. Thus, cells that migrate in an adhesion-independent 'amoeboid' migration mode might require cortex-driven forces for nuclear transit through narrow constrictions, or cells might benefit from an additional 'boost' from the cortex-driven pressure when pulling forces are insufficient to move the nucleus through a constriction. Other studies have indicated that deformation of the nucleus or collapse of the microtubule network in the rear compartment during confined migration might actively trigger contractility at the cell rear (Ju et al., 2023 preprint; Lomakin et al., 2020). Our work supplements these findings by demonstrating how contraction of the cell rear can push the nucleus forward to pass through constrictions. Future studies will be necessary to determine the specific factors determining the selection of a particular migration mechanism, and whether this is an active decisionmaking process requiring specific signaling pathways, or whether cells use multiple migration modes in parallel, with a specific mode dominating depending on the physical microenvironment (Wolf et al., 2013; Liu et al., 2015; Friedl and Wolf, 2010; Geum et al., 2016).

In conclusion, the recognition that myosin II- and Rho–ROCK-mediated rear cortex contraction aids in nuclear transit adds new insights into the mechanism by which cells traverse confining 3D environments, and further highlights the plasticity of cells to adapt their migration mode to the specific conditions. An improved understanding of the diverse mechanisms cells have available to overcome narrow interstitial spaces, and how cells select between these mechanisms, might lead to new targets for therapies to reduce or prevent cancer cell invasion and metastasis, or to boost the migration of immune cells to sites of infection.

MATERIALS AND METHODS

Cell culture

MDA-MB-231 metastatic breast adenocarcinoma cells were purchased from American Type Culture Collection (ATCC); HT1080 fibrosarcoma cells were a gift from Peter Friedl and Katarina Wolf (Radboud University Medical Center, Nijmegen, The Netherlands), originally purchased from DSMZ in Braunschweig, Germany; MEFs expressing GFP–Nesprin-2 were a gift from Cecile Sykes [Laboratoire de physique de l'ENS (LPENS), Paris, France]; MDA-MB-231 cells expressing the RhoA-FRET biosensor were a gift from Louis Hodgson (Department of Molecular Pharmacology, Albert Einstein College of Medicine, Bronx, New York, USA). All cell lines were cultured in Dulbecco's modified Eagle's medium (DMEM) supplemented with 10% (v/v) fetal bovine serum (FBS, Seradigm VWR), and penicillin and streptomycin (50 U/ml, Thermo Fisher Scientific) (denoted complete DMEM) and were maintained at 37°C and 5% CO₂. Cell lines were tested for mycoplasma infection following completion of experiments. Human cell lines were verified through the ATCC Cell Line Authentication Service.

Treatment with Rho and ROCK inhibitors and activators

For RhoA inhibition and activation experiments, cells were treated with Y-27632 ($10\,\mu\text{M}$; #1000583 Cayman Chemical), LPA ($10\,\mu\text{M}$; #L7260 Sigma Aldrich), RhoA Activator II ($1\,\mu\text{g/ml}$, #CN03 Cytoskeleton, Inc.) or a vehicle (DMSO) control for 4 h prior to start of each experiment.

Viral and piggybac modification

Cell lines were stably modified to express fluorescently tagged proteins using lentiviral vectors (pCDH-mCherry2-Actin Chromobody-puro and pCDHmNeonGreen-H2B Histone-puro). Transient expression of CMV-GFP-NMHC-IIA (Addgene #11347) and mCherry-MyosinIIB-N-18 (Addgene #55107) was achieved using a Nucleofector II electroporator and the Cell Line Nucleofector Kit V (Lonza Biosciences). MEFs and MDA-MB-231 cells were stably modified using BFP and DN-KASH expression plasmids in a doxycyclineinducible Piggybac plasmid backbone (Addgene #187019). For lentiviral modifications, pseudoviral particles were produced using 293TN cells (System Biosciences, SBI). The 293TN cells were transfected with the lentiviral plasmid of interest as well as lentiviral packaging and envelope plasmids (psPAX and pMD2.G, Addgene #12260 and #12259, respectively) using PureFection transfection reagent (SBI), per manufacturer's protocol. Supernatants were collected at 48-, 72-, and 96-h intervals post-transfection and passed through a 0.45 µm filter to remove cells and cellular debris. Cells to be transduced were cultured for 24 h prior to transduction at a confluency of 50% and were then cultured in lentivirus-containing medium with polybrene (8 µg/ml). Lentiviruscontaining medium was removed after 24 h, and following an additional 24 h of recovery time, cells were selected using 1 µg/ml of puromycin (Invivogen) for 3 days. For Piggybac modifications, MEFs were seeded into 6-well plates and were transfected with 1.75 µg of Piggybac plasmids and 0.75 µg of a hyperactive transposase using PureFection Transfection reagent (SBI), as per the manufacturer's protocol. Transfected cells were selected using 800 µg/ml G418 (Invivogen) for 3 days. Cells were sorted using flow-assisted cell sorting (FACS) in order to obtain consistent expression levels.

LINC complex disruption, and confirmation of nesprin displacement in MEFs and MDA-MB-231 cells

MEFs with fluorescently labeled endogenous nesprin-2 (GFP-Nesprin-2, Davidson et al., 2020) and expressing an mCherry2-actin chromobody and

either the inducible BFP-DN-KASH or BFP-only control construct were treated with 1 μ g/ml doxycycline for 24 h. Cells were subsequently fixed with 4% PFA for 15 min, washed with 1× PBS, and mounted on glass slides using Hydromount (Electron Microscopy Sciences).

For LINC complex disruption in MDA-MB-231 cells, cells expressing either the inducible BFP–DN-KASH or BFP-only control construct were treated with 1 μ g/ml doxycycline for 24 h. Cells were subsequently fixed with 1:1 methanol:acetone at -20° C for 15 min and washed with 1× PBS. Cells were then washed with 1× PBS and blocked in 3% BSA with 0.1% Triton X-100 (Thermo Fisher Scientific) and 0.1% Tween 20 (Sigma) in PBS for 1 h at room temperature. To confirm the displacement of endogenous nesprins, cells were immunofluorescently labeled with an antibody directed against human nesprin-1 [Developmental Studies Hybridoma Bank, MANNES1E(8C3), supernatant form] at a 1:3 dilution used overnight at 4°C. The following day, the cells were washed three times with 1× PBS and stained with Alexa Fluor 568 goat anti-mouse IgG1 secondary antibody (Life Technologies, cat. #A21124) at room temperature for 1 h. Coverslips were washed three times with 1× PBS and mounted on glass slides using Hydromount (Electron Microscopy Sciences).

Nesprin displacement was measured manually through observation of the GFP-Nesprin-2 signal using the ImageJ/FIJI software. Cells with high GFP-Nesprin-2 signal around the periphery of the nucleus were defined as 'non-displaced', whereas cells lacking this enrichment of GFP-Nesprin-2 at the nuclear envelope were defined as 'displaced' (see Fig.S3A,E). For doxycycline-treated cells, only BFP-positive cells were included for analysis. For cells that were not treated with doxycycline, all cells within the field of view were included in the analysis, as BFP expression requires doxycycline treatment. All analyses were conducted by an observer who was not aware of the test groups during the determination of nesprin displacement.

Microfluidic device preparation

Microfluidic devices were prepared as described previously (Davidson et al., 2015; Keys et al., 2018). Briefly, microfluidic devices were made through soft lithography by curing polydimethylsiloxane (PDMS) in a plastic mold containing microfluidic features at 65°C for 2 h. After removing cured PDMS from the mold, PDMS features were cut out using biopsy punches, and then both PDMS devices and glass coverslips were washed with deionized water and isopropyl alcohol, and then treated in a plasma cleaner (Harrick Plasma) for 5 min. PDMS pieces were then bound to activated coverslips and then heated at 95°C on a hotplate for 1 min to improve adhesion. After heating, devices were filled with 70% ethanol to sterilize internal surfaces, rinsed with PBS, and then coated with extracellular matrix proteins. For MDA-MB-231 cells, devices were coated with 50 µg/ml type-I rat tail collagen (Corning) in 0.02 M glacial acetic acid overnight at 4°C. For MEFs and HT1080 cells, devices were coated with 50 µg/ml fibronectin (Millipore) in PBS overnight at 4°C. Before seeding with cells, devices were rinsed once with PBS and once with cell media. Devices were then aspirated of all medium, and then loaded with cell-containing solution (roughly 20,000-30,000 cells per chamber). In devices, cells were cultured in Fluorobrite DMEM supplemented with 10% FBS (Seradigm, VWR), penicillin and streptomycin (50 U/ml, Thermo Fisher Scientfic), GlutaMAX and 10 mM HEPES (Gibco). Cells were allowed to attach within devices for 8–12 h before live-cell imaging. Cells were imaged for 12-14 h at 3-to-5-min intervals on a Zeiss LSM700 laser scanning confocal microscope at 37°C. For migration experiments with MEFs and MDA-MB-231 cells expressing either the inducible BFP-DN-KASH or BFP-only control constructs, the BFP channel was acquired using the 405-nm laser excitation line only at the beginning and end of each experiment to confirm BFP expression while minimizing phototoxic effects. Only cells expressing BFP-DN-KASH or BFP-only were used in the migration analysis.

Analysis of migration mode and nuclear transit times

Measurements of nuclear transit times were performed as described previously (Davidson et al., 2015). Briefly, cells were imaged at 5-min intervals on a Zeiss LSM710 laser scanning confocal microscope using 488-nm and 561-nm laser lines as they migrated through migration devices over a period of 12-16 h. A fluorescent marker of the nucleus (either

mNeonGreen–H2B histone, or GFP–Nesprin2) was used to track the position of the nucleus relative to microfluidic constrictions. An imaginary line was marked 5 μ m on either side of the middle of the constriction, to define when the nucleus 'enters' and 'exits' the constriction. The times at which the nucleus entered and passed through the constriction were noted, and this interval was recorded as the nuclear transit time. Cells which did not complete nuclear transit following entry to the constriction were excluded from analysis. These criteria were established prior to performing experiments, based on the prior work of our group with nuclear transit experiments.

Quantification of actin and myosin II localization

Quantification of fluorescent protein localization during nuclear transit was performed manually in the ImageJ/FIJI software package. The region of interest [i.e. rear cortex (RC), front cortex (FC), nuclear front (NF) or whole cell] was manually traced in the fluorescent channel of interest, and the average intensity of the fluorescent signal was measured (see Fig. S1). The rear cortex (RC) region was defined as a 2-µm-wide region starting at the rear perimeter of the cell, behind the nuclear constriction area. The front cortex (FC) region was defined as a 2-µm-wide region starting at the front perimeter of the cell, in front of the nuclear constriction area. The nuclear front (NF) region was defined as a 2-µm-wide region starting at the leading edge of the nucleus. The fluorescent signal was measured at a single time point during the specified stage of nuclear transit (i.e. 'Pre', 'Entry', 'Exit' or 'Post').

Collagen matrix cell migration assay

Collagen matrix cell migration assays were performed as described previously (Cross et al., 2010). In brief, PDMS wells were formed by punching out 10 mm diameter holes from PDMS slices. PDMS and glass coverslips were treated in a plasma cleaner for 5 min, before bonding PDMS to treated glass slides on a 95°C hot plate for 3 min. Wells were coated with 1% PEI (polyethyleneimine) for 10 min, followed by 0.1% glutaraldehyde for 30 min, and then subsequently washed with PBS once and cell medium once, before adding the collagen solution. Collagen matrices were prepared by mixing Type I rat tail collagen (Corning) with DMEM and NaOH (to reach a neutral pH of 7.4) with a solution of cells suspended in complete DMEM to achieve a final density of 80,000 cells/ml. Small volumes of collagen solution (10-15 μ L) were pipetted into the middle of wells, where they were allowed to polymerize at 37°C for 30 min. Following polymerization, wells were filled with complete DMEM and were subsequently incubated at 37°C for 48 h before imaging experiments.

RhoA FRET imaging and analysis

Analysis of RhoA-FRET biosensors was performed as described previously (Cheung et al., 2022). Cells were imaged at regular intervals on a dualchannel image acquisition set-up to minimize temporal and spatial misalignment problems, which impair FRET result interpretation. Cells were imaged at 5-min intervals for 12 to 16 h. Cells were excited with a ET436/20× (CFP excitation) source for an exposure time of 3 s with CFP excitation while CFP and YFP ('FRET') emission channels were captured simultaneously, by using a W-View Gemini beam splitter (A12801-01, Hamamatsu Photonics) and a T505lpxr dichroic mirror, through ET480/ 40 m and ET535/30 m optical filters, respectively. The light source for fluorescence imaging was a xenon arc lamp (Lambda LB-LS/30, Sutter Instruments). An absorptive neutral density filter with OD=0.3 (NE03B-A, ThorLabs) was used to attenuate light to minimize phototoxicity. All filters and dichroic mirrors were purchased from Chroma Technology. Prior to each experiment, the x-y positions of CFP and FRET channels were adjusted using the W-VIEW Adjustment software (Hamamatsu Photonics) to achieve a reasonable alignment for easier image registration and processing. The epifluorescence microscope was surrounded by an incubator with a temperature of 37°C, 5% CO_2 and humidity of ~70%.

Field alignment, flatfield correction and background subtraction were performed as described previously (Cheung et al., 2022). Images of cells were then manually masked by tracing the outline of cells using the CFP channel in ImageJ/Fiji. Following these corrections to both the CFP and FRET channels, FRET ratios were calculated by dividing the FRET channel

by the CFP channel. The sensitivity of the RhoA-FRET biosensor expressed in this MDA-MB-231 cell line to RhoA activation and inactivation was performed under identical experimental conditions on this imaging set-up as described previously (Cheung et al., 2022). Local FRET ratios were then calculated by manually tracing regions as defined in Fig. S4A.

Laser ablation of actin

Cells were seeded into migration devices 12–16 h before ablation experiments. Cells were maintained at 37°C in Fluorobrite DMEM containing 10% FBS, 10 mM HEPES (Gibco), GlutaMax, and penicillin and streptomycin (50 U/ml). Cells were imaged through a water immersion 40×/NA 1.1 objective (Carl Zeiss Imaging) using 488-nm and 561-nm laser lines. Cells were imaged at 3 s intervals for 63 frames. After 9 s, cells were ablated in defined regions using a 780 nm laser produced by a Spectra Physics Insight multiphoton excitation source. Ablation was performed at 40-70% attenuation, following ablation tests at the beginning of each experiment to verify that the laser successfully disrupted the actin cytoskeleton without causing cell death. Cells which exited the constriction, displayed rapid blebbing, or appeared to die following laser ablation were excluded from analysis, while cells which were able to recover following disruption of the actin network were included. Exclusion criteria were established prior to conducting experiments, based on prior experience with laser ablation assays (Mistriotis et al., 2019).

Image analysis of laser ablation experiments

Tracking of nuclear movement following laser ablation was achieved using ImageJ/FIJI software and a custom MATLAB script (available upon request). Briefly, the image channel containing the fluorescent mNeonGreen–H2B Histone signal was processed using a 3-pixel median filter to eliminate noise, and then a binary mask of this signal was generated using the built-in RenyiEntropy masking function in ImageJ/FIJI. This binary mask was then processed in MATLAB to track the position of the centroid of the nucleus at each time point. The furthest position of nuclear movement prior to recovery (within 20 s of the initial ablation) was considered to be the direct result of force disruption as a consequence of laser ablation and was recorded as the peak centroid shift (Fig. S5E). Bleb area measurements were performed in ImageJ/FIJI at the time point when the bleb had reached its maximum size. Outer bleb perimeter was traced manually, and inner bleb perimeter was traced at the periphery of the cell at the time point immediately prior to laser ablation.

Statistical analysis

All experimental data are based on at least three independent experiments, unless otherwise specified. Statistics tests were performed and graphs were created using GraphPad Prism (GraphPad Software, San Diego, USA). Nuclear transit times were compared using a one-way ANOVA with Sidak's post test. Frequency of nuclear transit mechanism selection and nesprin displacement analysis was performed using a χ^2 test of independence. Changes in local FRET ratio, actin accumulation, and myosin accumulation during nuclear transit were evaluated using a paired non-parametric one-way ANOVA test (Friedman). Nuclear centroid shifts following laser ablation were compared using an unpaired non-parametric one-way ANOVA test (Kruskal–Wallis). Bleb formation in cells ablated at a single site were compared using an unpaired non-parametric one-way ANOVA test (Kruskal–Wallis) while bleb formation in cells ablated at both cortexes simultaneously were compared using a paired non-parametric one-way ANOVA test (Friedman).

Acknowledgements

We thank Louis Hodgson for providing the MDA-MB-231 cell line expressing the RhoA-FRET Biosensor and Peter Friedl and Katarina Wolf for providing the HT1080 fibrosarcoma cell line. The mouse embryonic fibroblast cell line expressing Nesprin-2 GFP was made by Aude Battistella and Patricia Davidson and was a kind gift from Cécile Sykes and Sirine Amiri. We thank Klaus Hahn and Louis Hodgson for their advice regarding the use and analysis of FRET biosensors in migrating cells. We thank Philipp Isermann for his help in setting up the initial laser ablation experiments on MDA-MB-231 cells. We acknowledge the support of NYSTEM C029155 and National Institutes of Health (NIH) S10OD018516 grants and the help of the Cornell Institute of Biotechnology's BRC Imaging Facility (RRID:SCR_021741) for the use

of the Zeiss LSM880 inverted confocal microscope, which received funding through NYSTEM C029155 and NIH S10OD018516 awards for the Zeiss LSM880 inverted confocal microscope. We thank the Biotechnology Resource Center Flow Cytometry Facility (RRID:SCR_021740) for help with Flow Assisted Cell Sorting. This work was performed in part at the Cornell NanoScale Science & Technology Facility, a member of the National Nanotechnology Coordinated Infrastructure, which is supported by the National Science Foundation (award NNCI-2025233).

Competing interests

The authors declare no competing or financial interests.

Author contributions

Conceptualization: J.T.K., J.L.; Methodology: J.T.K., B.C.H.C., M.W., J.L.; Software: B.C.C.; Validation: M.A.E.; Formal analysis: J.T.K., B.C.H.C., M.A.E.; Investigation: J.T.K., B.C.H.C., M.A.E.; Resources: B.C.H.C., M.W., J.L.; Writing - original draft: J.T.K., J.L.; Writing - review & editing: B.C.H.C., M.A.E., M.W., J.L.; Visualization: J.T.K., B.C.H.C., J.L.; Supervision: M.W., J.L.; Project administration: J.L.; Funding acquisition: J.L.

Funding

This work was supported by awards from the National Institutes of Health (R01 HL082792, R01 GM137605, R35 GM153257, U54 CA210184 to J.L., R01 CA 221346 to M.W.) the Department of Defense Breast Cancer Research Program (Breakthrough Award BC150580 to J.L.), the National Science Foundation (CAREER Award CBET-1254846, URoL-2022048 to J.L., and Graduate Research Fellowships DGE-2139899 to M.A.E.), the Volkswagen Stiftung (A130142 to J.L.), and the Knight@KIC Engineering Graduate Fellowship (to J.K.). The content of this manuscript is solely the responsibility of the authors and does not necessarily represent the official views of the National Institutes of Health. Deposited in PMC for release after 12 months.

Data availability

All relevant data can be found within the article and its supplementary information.

Peer review history

The peer review history is available online at https://journals.biologists.com/jcs/lookup/doi/10.1242/jcs.260623.reviewer-comments.pdf

References

- Bone, C. R., Chang, Y. T., Cain, N. E., Murphy, S. P. and Starr, D. A. (2016). Nuclei migrate through constricted spaces using microtubule motors and actin networks in C. elegans hypodermal cells. *Development* 143, 4193-4202. doi:10.1242/dev. 141192
- Caille, N., Thoumine, O., Tardy, Y. and Meister, J. J. (2002). Contribution of the nucleus to the mechanical properties of endothelial cells. *J. Biomech.* 35, 177-187. doi:10.1016/S0021-9290(01)00201-9
- Charras, G. T., Yarrow, J. C., Horton, M. A., Mahadevan, L. and Mitchison, T. J. (2005). Non-equilibration of hydrostatic pressure in blebbing cells. *Nature* **435**, 365-369. doi:10.1038/nature03550
- Chen, M. B., Lamar, J. M., Li, R., Hynes, R. O. and Kamm, R. D. (2016). Elucidation of the roles of tumor integrin β1 in the extravasation stage of the metastasis cascade. *Cancer Res.* 76, 2513-2524. doi:10.1158/0008-5472.CAN-15-1325
- Cheung, B. C. H., Hodgson, L., Segall, J. E. and Wu, M. (2022). Spatial and temporal dynamics of RhoA activities of single breast tumor cells in a 3D environment revealed by a machine learning-assisted FRET technique. *Exp. Cell Res.* 410, 112939. doi:10.1016/j.yexcr.2021.112939
- Cross, V. L., Zheng, Y., Won Choi, N., Verbridge, S. S., Sutermaster, B. A., Bonassar, L. J., Fischbach, C. and Stroock, A. D. (2010). Dense type I collagen matrices that support cellular remodeling and microfabrication for studies of tumor angiogenesis and vasculogenesis in vitro. *Biomaterials* 31, 8596-8607. doi:10. 1016/j.biomaterials.2010.07.072
- Davidson, P. M., Denais, C., Bakshi, M. C. and Lammerding, J. (2014). Nuclear deformability constitutes a rate-limiting step during cell migration in 3-D environments. Cell Mol. Bioeng. 7, 293-306. doi:10.1007/s12195-014-0342-y
- Davidson, P. M., Sliz, J., Isermann, P., Denais, C. M. and Lammerding, J. (2015).
 Design of a microfluidic device to quantify dynamic intranuclear deformation during cell migration through confining environnments. *Integr. Biol.* 7, 1534-1546.
 doi:10.1039/C5IB00200A
- Davidson, P. M., Battistella, A., Déjardin, T., Betz, T., Plastino, J., Borghi, N., Cadot, B. and Sykes, C. (2020). Nesprin-2 accumulates at the front of the nucleus during confined cell migration. *EMBO Rep.* 21, e49910. doi:10.15252/embr.201949910
- Denais, C. M. Gilbert, R. M., Isermann, P., McGregor, A. L., te Lindert, M., Weigelin, B., Davidson, P. M., Friedl, P., Wolf, K. and Lammerding, J. (2016).

- Nuclear envelope rupture and repair during cancer cell migration. Science 352, 353-358. doi:10.1126/science.aad7297
- Doyle, A. D., Petrie, R. J., Kutys, M. L. and Yamada, K. M. (2013). Dimensions in cell migration. *Curr. Opin. Cell Biol.* 25, 642-649. doi:10.1016/j.ceb.2013.06.004
- Friedl, P. and Wolf, K. (2010). Plasticity of cell migration: a multiscale tuning model. J. Cell Biol. 188, 11-19. doi:10.1083/jcb.200909003
- Gadea, G., De Toledo, M., Anguille, C. and Roux, P. (2007). Loss of p53 promotes RhoA-ROCK-dependent cell migration and invasion in 3D matrices. *J. Cell Biol.* **178**, 23-30. doi:10.1083/jcb.200701120
- Geiger, F., Rüdiger, D., Zahler, S. and Engelke, H. (2019). Fiber stiffness, pore size and adhesion control migratory phenotype of MDA-MB-231 cells in collagen gels. *PLoS One* 14, e0225215. doi:10.1371/journal.pone.0225215
- Geum, D. T., Kim, B. J., Chang, A. E., Hall, M. S. and Wu, M. (2016). Epidermal growth factor promotes a mesenchymal over an amoeboid motility of MDA-MB-231 cells embedded within a 3D collagen matrix. *Eur. Phys. J. Plus* **131**, 8. doi:10. 1140/epip/i2016-16008-8
- Harada, T., Swift, J., Irianto, J., Shin, J.-W., Spinler, K. R., Athirasala, A., Diegmiller, R., Dingal, P. C. D. P., Ivanovska, I. L. and Discher, D. E. (2014). Nuclear lamin stiffness is a barrier to 3D migration, but softness can limit survival. *J. Cell Biol.* **204**, 669-682. doi:10.1083/jcb.201308029
- Hetmanski, J. H. R., de Belly, H., Busnelli, I., Waring, T., Nair, R. V., Sokleva, V., Dobre, O., Cameron, A., Gauthier, N., Lamaze, C. et al. (2019). Membrane tension orchestrates rear retraction in matrix-directed cell migration. *Dev. Cell* 51, 460-475.e10. doi:10.1016/j.devcel.2019.09.006
- Jayo, A. Malboubi, M., Antoku, S., Chang, W., Ortiz-Zapater, E., Groen, C., Pfisterer, K., Tootle, T., Charras, G., Gundersen, G. Â. G. et al. (2016). Fascin Regulates Nuclear Movement and Deformation in Migrating Cells. *Dev. Cell* 38, 371-383. doi:10.1016/j.devcel.2016.07.021
- Ju, R. J., Falconer, A. D., Dean, K. M., Fiolka, R. P., Sester, D. P., Nobis, M., Timpson, P., Lomakin, A. J., Danuser, G., White, M. D. et al. (2023). Compression-dependent microtubule reinforcement comprises a mechanostat which enables cells to navigate confined environments. bioRxiv 2022.02.08.479516. doi:10.1101/2022.02.08.479516
- Kalukula, Y., Stephens, A. D., Lammerding, J. and Gabriele, S. (2022). Mechanics and functional consequences of nuclear deformations. *Nat. Rev. Mol. Cell Biol.* 23, 583-602. doi:10.1038/s41580-022-00480-z
- Keys, J., Windsor, A. and Lammerding, J. (2018). Assembly and use of a microfluidic device to study cell migration in confined environments. In: *The LINC Complex: Methods and Protocols* (ed. G. G. Gundersen and H. J. Worman) pp. 101-118. New York, NY: Springer New York. doi:10.1007/978-1-4939-8691-0_10
- Khatau, S. B., Bloom, R. J., Bajpai, S., Razafsky, D., Zang, S., Giri, A., Wu, P.-H., Marchand, J., Celedon, A., Hale, C. M. et al. (2012). The distinct roles of the nucleus and nucleus-cytoskeleton connections in three-dimensional cell migration. Sci. Rep. 2, 488. doi:10.1038/srep00488
- Lammerding, J. (2011). Mechanics of the nucleus. Compr. Physiol. 1, 783-807. doi:10.1002/cphy.c100038
- Lämmermann, T., Bader, B. L., Monkley, S. J., Worbs, T., Wedlich-Söldner, R., Hirsch, K., Keller, M., Förster, R., Critchley, D. R., Fässler, R. et al. (2008). Rapid leukocyte migration by integrin-independent flowing and squeezing. *Nature* 453, 51-55. doi:10.1038/nature06887
- Lee, H., Alisafaei, F., Adebawale, K., Chang, J., Shenoy, V. B. and Chaudhuri, O. (2021). The nuclear piston activates mechanosensitive ion channels to generate cell migration paths in confining microenvironments. *Sci. Adv.* 7, eabd4058. doi:10.1126/sciadv.abd4058
- Liu, Y.-J., Le Berre, M., Lautenschlaeger, F., Maiuri, P., Callan-Jones, A., Heuzé, M., Takaki, T., Voituriez, R. and Piel, M. (2015). Confinement and low adhesion induce fast amoeboid migration of slow mesenchymal cells. *Cell* 160, 659-672. doi:10.1016/j.cell.2015.01.007
- Lomakin, A. J. Cattin, C. J., Cuvelier, D., Alraies, Z., Molina, M., Nader, G. PF., Srivastava, N., Sáez, P. J., Garcia-Arcos, J. M., Zhitnyak, I. Y. et al. (2020). The nucleus acts as a ruler tailoring cell responses to spatial constraints. *Science* 370, eaba2894. doi:10.1126/science.aba2894
- Lombardi, M. L. Jaalouk, D. E., Shanahan, C. M., Burke, B., Roux, K. J. and Lammerding, J. (2011). The interaction between nesprins and sun proteins at the nuclear envelope is critical for force transmission between the nucleus and cytoskeleton. J. Biol. Chem. 286, 26743-26753. doi:10.1074/jbc.M111.233700
- Marks, P. C. and Petrie, R. J. (2022). Push or pull: how cytoskeletal crosstalk facilitates nuclear movement through 3D environments. *Phys. Biol.* 19, 021003. doi:10.1088/1478-3975/ac45e3
- McGregor, A. L., Hsia, C. and Lammerding, J. (2016). Squish and squeeze-the nucleus as a physical barrier during migration in confined environments. *Curr. Opin. Cell Biol.* 40, 32-40. doi:10.1016/j.ceb.2016.01.011
- Mistriotis, P., Wisniewski, E. O., Bera, K., Keys, J., Li, Y., Tuntithavornwat, S., Law, R. A., Perez-Gonzalez, N. A., Erdogmus, E., Zhang, Y. et al. (2019). Confinement hinders motility by inducing RhoA-mediated nuclear influx, volume

- expansion, and blebbing. *J. Cell Biol.* **218**, 4093-4111. doi:10.1083/jcb. 201902057
- Pertz, O., Hodgson, L., Klemke, R. L. and Hahn, K. M. (2006). Spatiotemporal dynamics of RhoA activity in migrating cells. *Nature* 440, 1069-1072. doi:10.1038/ nature04665
- Petrie, R. J., Koo, H. and Yamada, K. M. (2014). Generation of compartmentalized pressure by a nuclear piston governs cell motility in a 3D matrix. *Science* **342**, 1062-1065. doi:10.1126/science.1256965
- Petrie, R. J., Harlin, H. M., Korsak, L. I. T. and Yamada, K. M. (2016). Activating the nuclear piston mechanism of 3D migration in tumor cells. *J. Cell Biol.* **216**, 93-100. doi:10.1083/jcb.201605097
- Poincloux, R., Collin, O., Lizárraga, F., Romao, M., Debray, M., Piel, M. and Chavrier, P. (2011). Contractility of the cell rear drives invasion of breast tumor cells in 3D Matrigel. *Proc. Natl. Acad. Sci. USA* 108, 1943-1948. doi:10.1073/ pnas.1010396108
- Ridley, A. J. Schwartz, M. A., Burridge, K., Firtel, R. A., Ginsberg, M. H., Borisy, G., Parsons, J. T. and Horwitz, A. R. (2003). Cell migration: integrating signals from front to back. Science 302, 1704-1709. doi:10.1126/science.1092053
- Rowat, A. C., Jaalouk, D. E., Zwerger, M., Ung, W. L., Eydelnant, I. A., Olins, D. E., Olins, A. L., Herrmann, H., Weitz, D. A. and Lammerding, J. (2013). Nuclear Envelope Composition Determines the Ability of Neutrophil-type Cells to Passage through Micron-scale Constrictions*. *J. Biol. Chem.* 288, 8610-8618. doi:10.1074/jbc.M112.441535
- Sahai, E. and Marshall, C. J. (2003). Differing modes of tumour cell invasion have distinct requirements for Rho/ROCK signalling and extracellular proteolysis. *Nat. Cell Biol.* 5, 711-719. doi:10.1038/ncb1019
- Schaar, B. T. and McConnell, S. K. (2005). Cytoskeletal coordination during neuronal migration. Proc. Natl. Acad. Sci. USA 102, 13652-13657. doi:10.1073/ pnas.0506008102
- Thiam, H. R., Vargas, P., Carpi, N., Crespo, C. L., Raab, M., Terriac, E., King, M. C., Jacobelli, J., Alberts, A. S., Stradal, T. et al. (2016). Perinuclear Arp2/3-driven actin polymerization enables nuclear deformation to facilitate cell migration through complex environments. *Nat. Commun.* 7, 10997. doi:10.1038/ncomms10997
- Thomas, D. G., Yenepalli, A., Denais, C. M., Rape, A., Beach, J. R., Wang, Y.-, Schiemann, W. P., Baskaran, H., Lammerding, J. and Egelhoff, T. T. (2015). Non-muscle myosin IIB is critical for nuclear translocation during 3D invasion. *J. Cell Biol.* **210**, 583-594. doi:10.1083/jcb.201502039
- Tinevez, J.-Y., Schulze, U., Salbreux, G., Roensch, J., Joanny, J.-F. and Paluch, E. (2009). Role of cortical tension in bleb growth. *Proc. Natl Acad. Sci. USA* 106, 18581-18586. doi:10.1073/pnas.0903353106
- Tsai, J. W., Lian, W. N., Kemal, S., Kriegstein, A. R. and Vallee, R. B. (2010). Kinesin 3 and cytoplasmic dynein mediate interkinetic nuclear migration in neural stem cells. *Nat. Neurosci.* 13, 1463-1472. doi:10.1038/nn.2665
- Wang, H., Alarcón, C. N., Liu, B., Watson, F., Searles, S., Lee, C. K., Keys, J., Pi, W., Allen, D., Lammerding, J. et al. (2021). Genetically engineered and enucleated human mesenchymal stromal cells for the targeted delivery of therapeutics to diseased tissue. *Nat. Biomed. Eng.* 6, 882-897. doi:10.1038/s41551-021-00815-9
- Weigelin, B., Bakker, G.-J. and Friedl, P. (2012). Intravital third harmonic generation microscopy of collective melanoma cell invasion. *Intravital* 1, 32-43. doi:10.4161/intv.21223
- Wilson, M. H. and Holzbaur, E. L. F. (2012). Opposing microtubule motors drive robust nuclear dynamics in developing muscle cells. J. Cell Sci. 125, 4158-4169. doi:10.1242/ics.108688
- Wolf, K., Mazo, I., Leung, H., Engelke, K., von Andrian, U. H., Deryugina, E. I., Strongin, A. Y., Bröcker, E.-B. and Friedl, P. (2003). Compensation mechanism in tumor cell migration: mesenchymal-amoeboid transition after blocking of pericellular proteolysis. *J. Cell Biol.* 160, 267-277. doi:10.1083/jcb.200209006
- Wolf, K. te Lindert, M., Krause, M., Alexander, S., te Riet, J., Willis, A. L., Hoffman, R. M., Figdor, C. G., Weiss, S. J. and Friedl, P. (2013). Physical limits of cell migration: control by ECM space and nuclear deformation and tuning by proteolysis and traction force. J. Cell Biol. 201, 1069-1084. doi:10.1083/jcb.201210152
- Wu, J., Lee, K. C., Dickinson, R. B. and Lele, T. P. (2011). How dynein and microtubules rotate the nucleus. J. Cell. Physiol. 226, 2666-2674. doi:10.1002/jcp. 22616
- Yadav, S. K., Feigelson, S. W., Roncato, F., Antman-Passig, M., Shefi, O., Lammerding, J. and Alon, R. (2018). Frontline science: elevated nuclear lamin A is permissive for granulocyte transendothelial migration but not for motility through collagen I barriers. J. Leukoc. Biol. 104, 239-251. doi:10.1002/JLB.3HI1217-488R
- Yamada, K. M. and Sixt, M. (2019). Mechanisms of 3D cell migration. *Nat. Rev. Mol. Cell Biol.* **20**, 738-752. doi:10.1038/s41580-019-0172-9
- Zhu, R., Antoku, S. and Gundersen, G. G. (2017). Centrifugal displacement of nuclei reveals multiple LINC complex mechanisms for homeostatic nuclear positioning. *Curr. Biol.* 27, 3097-3110.e5. doi:10.1016/j.cub.2017.08.073